Numerical and Experimental Investigations on Aerodynamic Behavior of the Ahmed Body Model with Different Diffuser Angles

P. Moghimi and R. Rafee[†]

Faculty of Mechanical Engineering, Semnan University, Semnan, Iran

[†]Corresponding Author Email: Rafee@semnan.ac.ir

ABSTRACT

Due to many restrictions applied by the necessity of fulfilling dimensional analysis in a numerical-experimental research and also the limits in experimental facilities a Low Reynolds Number simulation seems to be widespread. In this paper, effects of the diffuser angle on the aerodynamic behavior of the Ahmed body have been investigated for low Reynolds number flows. Numerical simulations were performed by solving the Reynolds Averaged Navier-Stokes (RANS) equations combined with different turbulence models. The Finite Volume Method (FVM) is used for simulations in Fluent 6.3.26 Software. The main objectives of the study are to improve the aerodynamic design of the body, analyzing the flow field to understand the nature of these improvements and reaching a suitable and reliable experimental-numerical setup for such a flow. Finally, it was concluded that the SST k-ω turbulence model with transitional flow corrections is the best choice. From the flow simulation and obtained experimental data, it was concluded that that drag coefficient is a function of three main phenomena. Results showed that the drag coefficient has its minimum value at a specific diffuser angle (8°) and further increases in the angle lead to higher drag coefficient. On the other hand, the lift coefficient constantly decreases by increasing the diffuser angle. In order to show the validity of the numerical results, experimental data were obtained by measuring the drag and lift coefficients of scaled standard Ahmed body and a model with the diffuser angle of 8 degrees in a wind tunnel. Results confirmed that improvement of drag and lift coefficients occurs when diffuser region is considered for the Ahmed body. In addition, the flow field around the body was studied in detail to show the effects of the diffuser geometry on the aerodynamic characteristics of the body.

Keywords: Lift Coefficient; Drag coefficient; Diffuser angle; Ahmed body; Low Reynolds Number flow.

1. INTRODUCTION

The vehicle aerodynamics was started in the 20th century. Needs for higher speeds and faster transportations with low fuel consumptions led the designers to study the vehicle aerodynamics to achieve better technical efficiency (Hucho, 1987). This goal could be achieved by the comprehensive study of flow topologies around the body leading to optimization of the global shape and use of flow control devices. Many active and passive methods have been brought into the field to obtain aerodynamic optimizations that will be mentioned in the literature.

The aerodynamic coefficients of lift and drag have a great influence on vehicles technical parameters (e.g. fuel consumption, handling, road stability, passenger comfort etc.). Drag coefficient directly affects fuel consumption and engine's maximum power needed. The lift coefficient affects the vehicle's stability and handling (Katz, 1947). The

diffuser is widely used for sports cars and plays a vital role in the aerodynamic performance of the vehicle. Since diffuser is considered beneath the vehicle, it will not affect the car appearance. In this research, a simplified car model called "Ahmed body" is considered to investigate "how diffuser affects aerodynamics?"

Ahmed *et al.* (1984) introduced the "Ahmed body" in 1984. Their study focused on the effects of slant angle on the body's drag coefficient. They examined the changes of drag coefficient with the variation of slant angle in the range of 0 to 40 degrees. A comprehensive study of the wake structure behind the Ahmed model was done by Lienhart *et al.* (2000). It was concluded that by increasing the slant angle up to 12.5^o, the drag decreases. Beyond this optimal value, the drag increases and reaches its maximum value at the slant inclination of 30°. Sudden decreases in drag were observed by the further increase in the inclination. For inclinations lower the critical angle

(close to 30°), the flow remains attached to the rear window and longitudinal counter-rotating vortices are formed at the edges. The intensity growth of these stream-wise vortices directly leads to drag increase. On the other hand, above the critical angle flow separation occur at the leading edge of the rear window and accordingly forms massive recirculation regions (Ahmed *et al.* 1984 and Lienhart *et al.* 2000). After that many studies have been performed to investigate the flow topologies around the Ahmed model. Since the low-pressure regions of the body are responsible for a large proportion of pressure drag, most of the studies focused on the wake structure behind the geometry. Bayraktar *et al.* (2001) studied the influence of Reynolds number on the drag and lift coefficients of the Ahmed body. It was concluded by increasing the Reynolds number from 2.2M to 13.2M, drag coefficient increases while lift coefficient is nearly constant. Beaudion *et al.* (2004) studied the pressure coefficient around the Ahmed body in a cavitation fluid flow. It was concluded that the pressure coefficient of longitudinal vortices formed because of the flow separations at the slant angle in which $C_p = -1.67$, which shows the vital role of these vortices on the drag coefficient. Recently, Minguez *et al.* (2009) and Rajsin *et al.* (2012) performed experimental and numerical studies on the external flow and turbulent wake structures around the Ahmed body. Minguez *et al.* (2009) used spectral vanishing viscosity LES (SVV-LES) method. His formulation needed no additional computational cost of the SVV-LES with respect to DNS. Rajsin *et al.* (2012) used Spalart-Allmaras turbulence model and concluded this turbulent model could not predict the flow over the slant well at high Reynolds numbers.

Since the fuel consumption has become more important over the last few decades, many studies were performed on the reduction of the drag coefficient. For example, Khaled *et al.* (2012) studied a simplified car model with air inlets and outlets including a real cooling system and a simplified engine block. Their configurations could decrease drag and lift coefficient by 2% and 5% and aerodynamic cooling coefficient by 50% respectively. Rohatgi (2012) employed some instruments like a rear screen, rear fairings, and vortex generators that resulted in the drag reduction up to 6.5%, 26% and 1.24%, respectively. Sonawane *et al.* (2011) showed that changing the slant angle of an Ahmed body from 30° to 20° could decrease the drag up to 8% and a 1.5 to 5% save on fuel consumption. The aerodynamic behavior of Ahmed body is studied experimentally and numerically by Castro *et al.* (2010), considering the pressure distribution and drag coefficient of the body. They showed the importance of the stilts by experiments and simulations. Strachan *et al.* (2004 and 2007) investigated the effect of moving ground on the flow structure around the body using LDA technique. The results showed that the ground movement decreases the size and strength of the vortex shedding behind the Ahmed body. It is worth mentioning that considering ground movement is important because in the real situation when the vehicle moves on the road, there is not any relative motion between the air and the ground so boundary layer does not form. Mack *et al.* (2012) studied ground simulation upgrades of a wind tunnel. It was shown that a moving ground could be implemented successfully as an independent system in their under–study wind tunnel in spite of tough criteria needed to be met. Hui *et al.* (2006) showed that diffuser angle and the ground clearance of the body can effectively change the diffuser performance. Kato *et al.* (1997) investigated the relation between the locations of the obstacles attached to the underbody and the change in drag. Computational results proved that the drag tends to increase when the obstacle is located around the front axle or behind the rear axle. They suggested an improved underbody shape to reduce the drag. Cogotti (1998) investigated the influence of geometry variations that affect the underbody flow field. He studied three different diffuser angles. Although it could not be considered as a comprehensive benchmark for realizing how considering a diffuser affects the aerodynamic characteristics, it shows the great influence of diffuser angle variation on the drag coefficient. Howell (1994) studied the influence of moving ground on the aerodynamics of simplified car models with diffusers. The results revealed that for most aerodynamic development in the conventional wind tunnels, utilizing fixed ground is adequate except for optimizations which can influence the airflow around the wheels. Cederland *et al.* (2010) investigated the influence of Rim design on a sports car model and its influence on the wing and diffuser flow. Results showed that covering the front and rear wheels increases downforce. Even a drag reduction observed by covering the front wheel. Also, they concluded that removal of the lower wing reduces the size of base wake which drives flow through the diffuser to a great extent. Grandemange *et al.* (2013b and 2014) controlled the separated flow past Ahmed body using flaps at the top and bottom trailing edges of the body. An optimized geometry, in terms of drag reduction up to 5.8%, reported to be $\Phi_T = 9.2^o$ for the top flap and $\Phi_B = -7.4^o$ for the bottom flap for inclinations. It was concluded that the optimal slant angle is depended on the bottom flap orientation and the optimization of drag cannot be achieved by individual optimization of each angle. Bruneau *et al.* (2014) studied the methods that could decrease low-pressure region behind the Ahmed body resulted from generated vortices behind the body. It was proved that this low-pressure depend on two parameters; the distance of the vortex to the wall and its amplitude (circulation). It resulted that there are two ways that can reduce this pressure drag: 1. An active control procedure by use of pulsed jet and 2. A passive control method using porous layers that change the vortex shedding. It was concluded that coupling the two control techniques results in a drag reduction up to 31%. Some other passive methods have been investigated by Wang *et al.* (2016). He experimentally investigated the effects of deflectors on the aerodynamic drag and near

wake of Ahmed body with a 25° slant angle. It was evidenced that mounting deflectors at the side edges of the slant can have different effects. For the deflector height $H_D / l = 1\%$ (l is the model length), the drag increased up to 2.1% Nevertheless, higher values of $H_D / l = 2\%$ and 3% led to drag reductions up to 3.9% and 7.6% respectively. Also, it was concluded that considering the deflector at the slant leading edge can be more efficient which lead to drag reductions up to 9.3%, 10.7% and 10.9% for deflector width of 1% 2% and 1% of 3% respectively which shows the inevitable effect of deflectors on the downstream flow field. In 2014, Tunay *et al.* investigated the flow field downstream the Ahmed body with various slant angles (25° 30° and 35°). It was observed that there are three mainly critical flow points in the wake downstream of the body and changing the inclination of the slant angle, leads to changes in the locations of these points. In addition, the dependence of Ahmed body flow structure on aspect ratio (AR) has been studied by Corallo *et al.* (2015). The aspect ratio in this is study is defined as "cross-sectional aspect ratio of Ahmed model to cross-sectional aspect ratio of the standard-dimension Ahmed". Aspect ratios between 0.6 and 1.6 were simulated in increments of 0.1. It was found that flow interaction over the slant with longitudinal vortices, significantly changes the critical slant angle. Hu *et al.* (2011) investigated the influence of diffuser angle on the lift and drag coefficients of a simplified car model numerically. In addition, the influences of diffuser angle and ground clearance on the drag coefficient were studied numerically and experimentally on a simplified car model by Lai *et al.* (2011). Both of these researches concluded that there is an optimum inclination for diffuser angle at $\alpha = 9.8^o$ for Hu *et al.* (2011) where *Lai et al.* (2011) found the optimum angle at $\alpha = 8^o$, $\alpha = 12^o$ and $\alpha = 8^o$ for ground clearances of $D = 20mm$, $D = 25mm$ and $D = 30mm$ respectively which emphasizes the vital effect of ground clearance in assigning the optimum angle. Also a descending behavior for lift coefficient has been stated by Hu *et al.* (2011) while the diffuser angle increases. Huminic *et al.* (2010 & 2012) studied some underbody geometry effects on a 35° slant angle Ahmed body Aerodynamic numerically. Focusing the front radius of the front section, angle and length of the diffuser, an approach was provided by the authors to evaluate the contribution of the underbody to the total drag. From the diffuser angle point of view, it was concluded that by increasing the diffuser angle, downforce increases while drag behavior is predictable for angles up to $\alpha_d = 7^o$ due to intensive flow separations starting beyond this angle. Also, Aulakh (2016) investigated the effect of diffuser angle on the Aerodynamic drag of two Ahmed bodies in convoy. It was observed that up to certain diffuser angles the average drag of convoy is lesser than that of the case with no diffuser because of the axial vortices produced by the leading body's

diffuser.

Due to many restrictions applied by the necessity of fulfilling dimensional analysis in a numerical-experimental research and also the limits in experimental facilities (Not always an ideal full-scale Wind tunnel is reachable), such a case (Low Reynolds Number) seems to be widespread. So this research was performed to make a comprehensive study while bringing experimental tests into account on the effects of diffuser angle on the flow field around the Ahmed body, drag and lift coefficients facing a low Reynolds number challenge to help engineers with their design challenges to find out that how can diffuser affect aerodynamics? The diffuser is particularly interesting since it corresponds to a common aerodynamic add-on device applied by car manufacturers on real sports cars. For this purpose, both of numerical and experimental data were presented and analyzed. In the previous studies that include the investigation of diffuser angle effect on the aerodynamic coefficients (See e.g. Hu *et al.* (2011) and Lai *et al.* (2011)) for specific models, the reasons for the aerodynamic behavior haven't been presented properly and completely. This became the motivation and objective behind conducting the present study. So in this study, the aerodynamic phenomena and flow structures resulted from adding diffuser have been brought into focus to answer questions like: How can diffuser help to improve aerodynamics? How can it influence the flow domain behind the body? Furthermore, authors have tried to reach a reliable experimental-numerical setup for such studies (Low Reynolds Number experimental and numerical simulations) by means of the data presented in the literature and their own trial and errors which is the advantage of the present work in comparison with related references (Hu *et al.* (2011), Lai *et al.* (2011), Huminic *et al.* (2010 & 2012) and Aulakh (2016)).

2. PROBLEM DEFINITION

The diffuser which is shown in Fig. 1 has a slope of the trailing of the under body and has a great effect on vehicle aerodynamics. The air flow around a vehicle is complex, three dimensional and turbulent. It is significantly affected by the flow separations. The difference between vehicles and flying bodies' aerodynamics is the ground effect which has a great effect on the flow field around the vehicle (Hucho 1987). So it is important to take this effect into account. Figure 2, shows the geometry of standard reference Ahmed body and dimensions introduced by Ahmed *et al.* (1984). In spite of neglecting a number of features of a real car (rotating wheels, rough underside, etc.), necessary flow characteristics could be generated (like flow separations, wake region behind the body and etc.). Although the slant angle (φ see Fig. 2) is variable, in this study the inclination of the slant angle is fixed at $\varphi = 25^o$ which is common in studies (Lienhart *et al.* (2000), Meile *et al.* (2010), Tunay *et al.* (2014), and etc.) Figure 3, represents the two main design parameters of a diffuser, namely

diffuser angle (α) and diffuser length (L) on the Ahmed body geometry. In this research, the diffuser length is considered to be constant and the aim is to investigate the influence of diffuser angle variation on aerodynamic behavior.

Limiting factors are the laboratory's environmental conditions, dimensions of the wind tunnel and the wind tunnel capabilities (like the flow speed). So in order to achieve the similarity between experiments and numerical simulations, the experimental conditions have been considered as the base for defining the parameters in the numerical simulations. Dimensions of the wind tunnel, boundary conditions (velocity of flow, the density of air), and the model dimensions are implemented in the simulations.

Fig. 1. Diffuser region under a sample car.
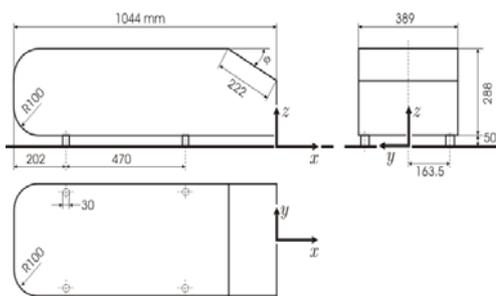
Fig. 2. Standard Ahmed body geometry (all dimensions in mm), Ahmed *et al.* (1984).
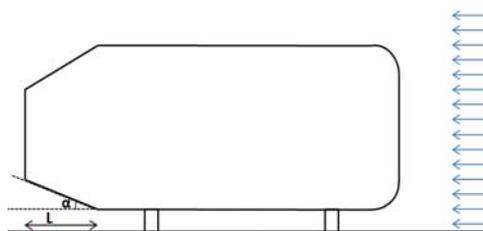
Fig. 3. Diffuser angle (α) and length (L) on the geometry, Flow direction over the body shown by parallel arrows.

Variations of the aerodynamic behavior are studied by simulation of the flow around the standard Ahmed body and models with diffuser angles of 4, 8, 12, 16 and 20 degrees. Experiments were performed on the standard model and the model with optimum diffuser angle of 8 degrees in the wind tunnel.

3. RESEARCH APPROACH

The models of the Ahmed body were studied with the scale of 1:10 (both numerical and experimental simulations) because of the limits in wind tunnel dimensions and the necessity of fulfilling the

conditions of similarity in dimensional analysis. The main restriction is the "blockage ratio". This ratio is defined as the ratio of model frontal area to the wind tunnel test section area. This criterion is defined in order to make sure that wind tunnel walls would not affect the flow field around the body significantly. Hucho (1987) and Wang *et al.* (2013) have declared that the maximum acceptable value for this ratio 5 percent. In this study, the blockage ratio is 2.6%, which fulfills the criterion.

The optimum diffuser angle is the angle at which the drag coefficient has its minimum value. The standard model and the model with optimum diffuser angle were tested in the wind tunnel in order to validate the results of numerical simulation.

3.1 Numerical Simulation

3.1.1 Turbulence Model

In this research, the numerical simulation has been conducted using the Fluent 6.3.26. Different turbulence models were examined and the "SST k-ω" model was chosen for simulations. According to the model dimensions and the maximum speed of the flow in the wind tunnel, the Reynolds number of the flow was $Re = 9.31 \times 10^4$ based on model's length. The Shear Stress Transport k-ω model which is a suitable model for low Reynolds numbers has been chosen. This model can effectively blend the robust and accurate formulation of the k-ω model (which works well in the near wall region) with the free-stream characteristics of the k-ε model (which is good at the far field) (Fluent 2015). In addition, the "Transitional Flows" option is enabled in the software to add the low Reynolds number corrections to the simulations.

3.1.2 Governing Equations

The flow field around the body has been simulated by solving appropriate governing equations such as conservation of mass (1) and momentum (2). The first equation is used to calculate velocity in flow domain and the momentum is needed to calculate forces related to the speed changes. Bringing turbulence into the field, the transport equations of turbulence kinetic energy, k (3), and the specific dissipation rate, ω (4) (Fluent 2015) have been used. "k" is characterized by measured root-mean-square (RMS) velocity fluctuations and the term "ω" represents the rate at which turbulence kinetic energy is converted into thermal internal energy per unit volume and time.

$$\frac{\partial \rho}{\partial t} + \frac{\partial}{\partial x_i}\left(\rho \bar{u}_i\right) = 0 \tag{1}$$

$$\frac{\partial \rho}{\partial t}\left(\rho \bar{u}_i\right) + \frac{\partial}{\partial x_j}\left(\rho \bar{u}_i \bar{u}_j\right) =$$
$$-\frac{\partial \bar{P}}{\partial x_j} + \frac{\partial}{\partial x_j}\left(-\rho \overline{u_i' u_j'}\right) \tag{2}$$
$$+ \frac{\partial}{\partial x_j}\left[\mu\left(\frac{\partial \bar{u}_i}{\partial x_j} + \frac{\partial \bar{u}_j}{\partial x_j} - \frac{\tau}{\tau}\delta_{ij}\frac{\partial \bar{u}_k}{\partial x_k}\right)\right]$$

$$\frac{\partial}{\partial t}(\rho k) + \frac{\partial}{\partial x_i}(\rho k \overline{u}_i) = \frac{\partial}{\partial x_j}\left(\Gamma_k \frac{\partial k}{\partial x_j}\right) \\ + \widetilde{G_K} - Y_K + S_K \quad (3)$$

$$\frac{\partial}{\partial t}(\rho \omega) + \frac{\partial}{\partial x_i}(\rho \omega \overline{u}_i) = \frac{\partial}{\partial x_j}\left(\Gamma_\omega \frac{\partial k}{\partial x_j}\right) \\ + G_\omega - Y_\omega + D_\omega + S_\omega \quad (4)$$

Terms "ρ", "$\overline{u}$", "P" represent the flow density, mean velocity and pressure respectively. $\widetilde{G_K}$ is the generation of turbulence kinetic energy due to mean velocity gradients and the G_ω is the generation of ω. Γ_k and Γ_ω are the effective diffusivities of k and ω. The terms Y_K and Y_ω are the dissipation of the k and ω due to turbulence. S_K and S_ω represent the user-defined source terms. Also, D_ω is the term related to the cross-diffusion. The Reynolds stress term, $\left(-\rho \overline{u_i' u_j'}\right)$ in the Eq. (2), represents the effects of turbulence and time-averaged variables. Fluent employs the Boussinesq Approach to appropriately model this term which is defined as:

$$-\rho \overline{u_i' u_j'} = \mu_t\left(\frac{\partial \overline{u}_i}{\partial x_j} + \frac{\partial \overline{u}_j}{\partial x_i}\right) - \frac{2}{3}\left(\rho k + \frac{\partial \overline{u}_k}{\partial x_k}\right)\delta_{ij} \quad (5)$$

Where the term μ_t, stands for the turbulent viscosity.

3.1.3 BOUNDARY CONDITIONS

Table 1 shows the boundary conditions employed in the simulations based on real experimental setup.

3.1.4 GEOMETRY OF THE PROBLEM AND MESH GENERATION

Since the studied model has been symmetric and neglecting the effects of side winds, the flow was considered to be symmetric (Hu *et al*. 2011) and only half of the body was considered in the simulations in order to decrease the simulation time. Positioning the Ahmed body in the wind tunnel is in accordance with the suggestion of Manceanu and Bonnet (2002) in the manner that wind tunnel dimensions won't affect the flow around the body significantly (Fig. 4).

Gambit 2.4.6 software was used for grid generation with tetrahedral cells. Because of the formation of the boundary layer on the body and the importance of boundary layer flow simulation on the body, the mesh used near the body has been generated smaller. But at the domain far from the model, meshing with larger size has been used in order to decrease the amount and time of calculations.

3.1.5 Numerical Solution Controls

In the simulations, a coupled pressure-velocity coupling has been used. Also, the second order upwind method is used to discretize the convective terms of the transport equations for momentum, turbulent kinetic energy and specific dissipation

Table.1 Boundary Conditions.

Condition	Data	Statement
Fluid : Air	$\rho = 1.0478$ [kg/m^3]	Laboratory condition
Velocity Inlet	V=16[m/s]	Wind tunnel speed
	D_H= 0.3 [m]	D_H= Model hydraulic diameter
Pressure Outlet [abs]	P=88780[Pa]	Measured at laboratory condition
Symmetry plane	symmetric	According to flow domain symmetry
Walls	No slip condition	Boundary layer formation
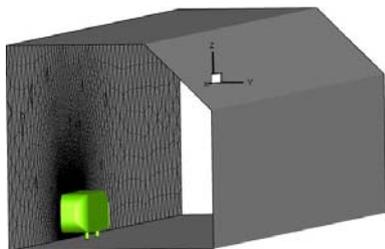
Fig. 4. Geometry of the problem based on real experimental setup

rate. The pressure-based solver was chosen and an implicit formulation has been used for simulations. The flow is considered to be steady and

convergence criterion of 10^{-6} for residuals is considered for termination of iterations for both the continuity and velocity components, 10^{-5} for k and ω and changes smaller than 1% in aerodynamic coefficients.

3.2 Experimental Setup

An open-loop wind tunnel (see Fig. 5) is used for experimental testing of the models. The wind tunnel specifications are represented in Table 2 and Fig. 6, shows the model and ground plane in the wind tunnel.

As mentioned before, the Reynolds number is low ($Re = 9.31 \times 10^4$) It is expected that the transition

from laminar to turbulent in the flow would not occur. An attempt was made to make the flow turbulent by creating sharp edges at the leading edges of the model as suggested by Wang *et al.* (2013). A plastic layer was stuck on the model (see Fig. 7). This layer can decrease the wooden model roughness as well.

Fig. 5. Open loop wind tunnel.

Table 2 Wind Tunnel Specification.

Length of the test section [cm]	50
Area of the test section [cm²]	1623.76 (Without ground plane)
Operating Speed [m/s]	16
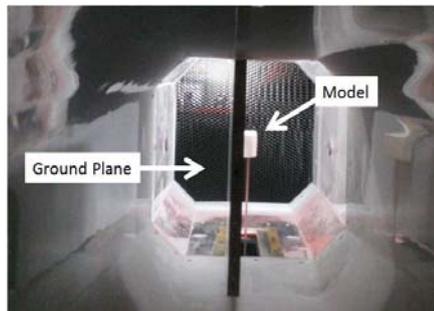
Fig. 6. Model and the ground plane position in the test section, Rear view of the test section.

(a)
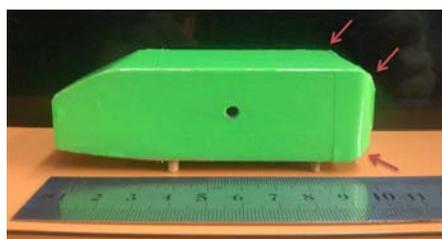
(b)

Fig. 7. (a): Wooden model with the scale of 1:10 (b): plastic layer applied to the model - forming sharp edges at the front of the model (shown by arrows).
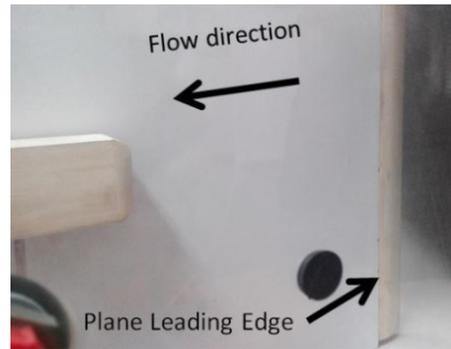
Fig. 8. Creating a leading edge with a sharped profile in order to prevent flow separations at the beginning of the ground plane.

As mentioned before simulating the ground effect is inevitable. So a plane is used in the middle of the test section in order to simulate the ground effect. This plane must be sharp at the leading edge to prevent the flow separations at the beginning of the plane (See Fig. 8).

Measurements of the lift and drag forces have been conducted by a simple balancing system. One of the most important points of measurements is the fact that the measurement system showed the forces of body and the strut both together. So the measurements of the strut forces must be done separately and the models' net force is the difference between these forces. Additionally, the uncertainty of the measurements is represented in the results (see Table 5). It was observed that measured velocity and forces cause more uncertainty than other factors such as air density and model dimensions.

Checking the repeatability of the measurements, the experiments where repeated at least 10 times for each case. The results recorded in Table 5 are the average of the measured data for each model.

4. VALIDATION OF THE NUMERICAL SIMULATION

At the first step, the results of numerical simulations for standard Ahmed body was compared with the results of a simulation done by Meile *et al.* (2010) that applied the Reynolds Stress Model (RSM) with the flow velocity of 40 m/s to ensure that the employed boundary conditions, meshing, geometry generation, solving method and calculated coefficients by the software are valid and suitably chosen. Results of this validation, that were reasonably accurate, are presented in table 3.

Some other models such as RNG k-ε model were used at the beginning of the simulation phase of this study. Many of the tested turbulence models were appropriate for flows with high Reynolds numbers (Fluent 2015) and could not predict suitable results for tested velocities in our experimental setup. In addition, results for different models were quite different in some cases. As an example, the SST k-ω model predicted flow separation at the Ahmed body's slant angle (See Fig. 9 a) while this

separation was not predicted by the RNG k-ε (Fig. 9b). The Spalart-Allmaras model was chosen to judge this difference which is a capable model of predicting low Reynolds number flow topologies. As could be observed (Fig. 9c) this model confirmed the separation too.

Table 3 Validation of Numerical Simulation Approach with Meile *et al.* (2010) (both studies at Re = 2.78×10^6).

Study	Turb.model	Drag coefficient	Lift coefficient
Meile *et al.* (simulations)	RSM	0.295	0.387
Meile *et al.* (experiments)	-	0.299	0.345
Present work (simulation)	SST k-ω	0.298	0.364

Table 4 Checking the Grid Independency of the SST k- ω model Solution.

No. of cells (million)	Coefficient		No. of cells (million)	Coefficient	
	Drag	Lift		Drag	Lift
α=0º			α=4º		
2.56	0.411	0.269	2.71	0.386	0.071
2.73	0.412	0.226	2.91	0.386	0.075
error	0.24%	19%	error	0%	5.6%
α=8º			α=12º		
3.23	0.382	-0.040	3.40	0.385	-0.134
3.43	0.382	-0.043	3.64	0.385	-0.135
error	0%	7.5%	error	0%	0.74%
α=16º			α=20º		
3.84	0.387	-0.142	4.02	0.387	-0.163
4.01	0.388	-0.144	4.20	0.388	-0.165
error	0.25%	1.4%	error	0.25%	1.2%

(a)

(c)
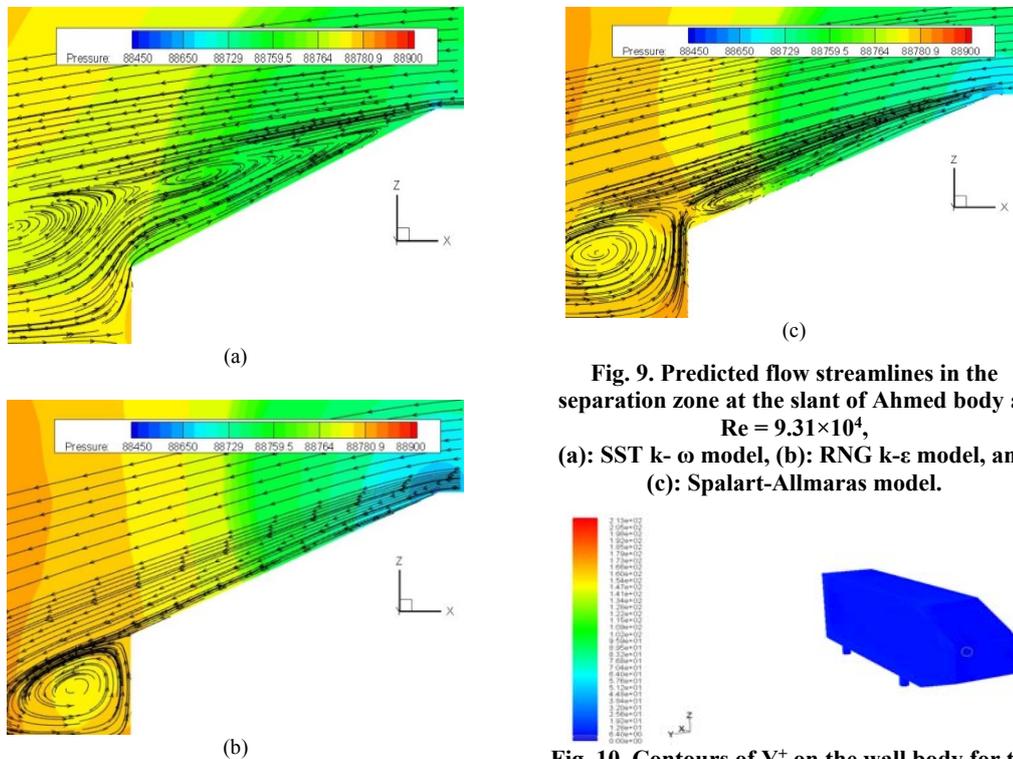
Fig. 9. Predicted flow streamlines in the separation zone at the slant of Ahmed body at Re = 9.31×10^4, (a): SST k- ω model, (b): RNG k-ε model, and (c): Spalart-Allmaras model.

(b)
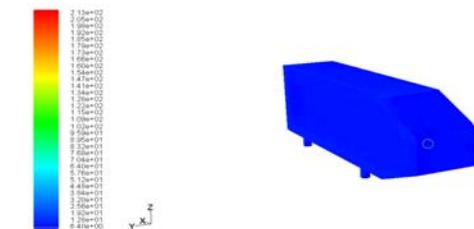
Fig. 10. Contours of Y$^+$ on the wall body for the final Turbulence model selected in the study (SST k-ω model with the Transitional Flows).

So finally the SST k-ω with transitional flows option has been chosen as the turbulence model in this research. In addition, the Transitional Flows option has been employed to apply the low Reynolds corrections on the turbulent viscosity.

To examine the quality of mesh generation, the results of grid independence test have been presented in table 4. In addition, as reported by Fluent 6.3.26 User Guide, for the SST k-ω model if the Transitional Flows option is used in the simulations, the y^+ should be in the order of unity. However, a higher y^+ is acceptable if the first cells were located inside the viscous sublayer ($y^+<4$ to 5). Figure 10 shows the contours of y^+ on the wall body. It shows the suitability of the meshes near the solid walls.

The comparison between the experimental and numerical results for two different Ahmed body models (the standard model and the model with the optimum diffuser angle of 8 degrees) is presented in table 5. It can be seen that the experimental data, confirm the behavior of the drag and lift coefficients obtained from the simulations. It worth mentioning that the case with almost 25% error is related to the negative lift. Because of placing ground plane under the body, measuring the negative lift needed a practical method. The negative lift has been measured by setting the zero point of measurement system at a positive value. While meeting the expected conditions in the tunnel (steady state), the lift shown by measurement system reached zero value. The decreased value of lift was considered to be the negative lift. This trial and error method has been utilized to measure the negative lift which looked to be the most accurate one as shown by authors' experiences in this study.

Qualitative validations were done by Hu *et al.* (2011) and Lai *et al.* (2011). They investigated the influences of the diffuser angle on the aerodynamic coefficients of lift and drag for simplified car models. The results of their study show that there is an optimum diffuser angle at which the drag coefficient has its minimum value and descending behavior for lift coefficient as the diffuser angle increases which is reasonably in agreement with the results of the present study (Figs. 11 (a) and (b)).

Table 5 Experimental and Numerical Results for Diffuser Angles of 0 and 8 Degrees.

Coeff.	Numerical results (SST k- ω)	Experimental results	Error %
Standard model ($\alpha = 0°$)			
(C_d)	0.412	0.449 ± 0.04	8.3
(C_L)	0.226	0.257 ± 0.03	12.1
Optimum model ($\alpha = 8°$)			
(C_d)	0.382	0.417 ± 0.04	6.8
(C_L)	-0.040	-0.032 ± 0.03	24.7
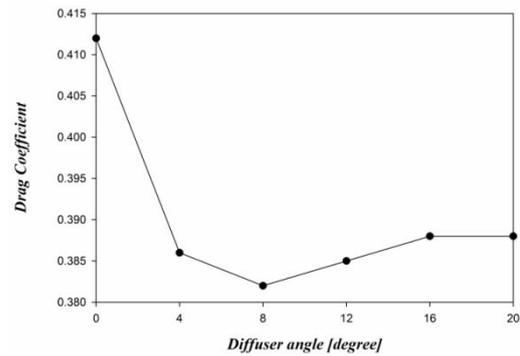
(a)
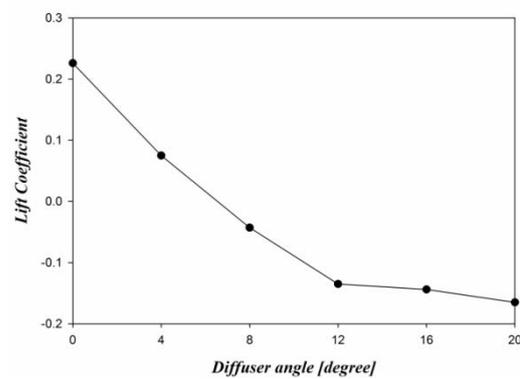
(b)

Fig. 11. Variations of the lift and drag coefficient vs. diffuser angle (a): Drag coefficient (C_d), (b): Lift coefficient (C_L).

Also, recently some new studies have been conducted numerically to investigate the Ahmed body's diffuser effects on the Aerodynamics. The quantitative behavior predicted by these studies are suitably in agreement with the present study as well (see Huminic *et al*. (2010&2012) and Aulakh *et al*. 2016).

5. RESULTS AND DISCUSSION

5.1 Drag Coefficient

Figure 11, shows the results of CFD simulations. In Fig. 11(a) the variations of drag coefficient versus diffuser angle changes is shown. As can be seen, at the diffuser angle of 8 degrees, the drag coefficient reaches its minimum value. However, the further increase in diffuser angle leads to higher drag coefficients. Diffuser angle of 8 degrees is considered to be the optimum angle for drag coefficient.

After studying the flow pattern around the body it was concluded that the drag coefficient is significantly affected by three dominant phenomena. These factors seemed to be: a) Low-pressure recirculation regions behind the body, b) flow separation in the diffuser and c) longitudinal vortices formed at the side edges of the diffuser.

To verify the size of the low-pressure regions

behind the body, the flow pattern has been checked in the symmetry plane (See Fig. 12). The recirculation regions show the low-pressure areas in which the flow loses its energy and so the pressure decreases. It can be seen that the core of this

(a)

(b)

(c)
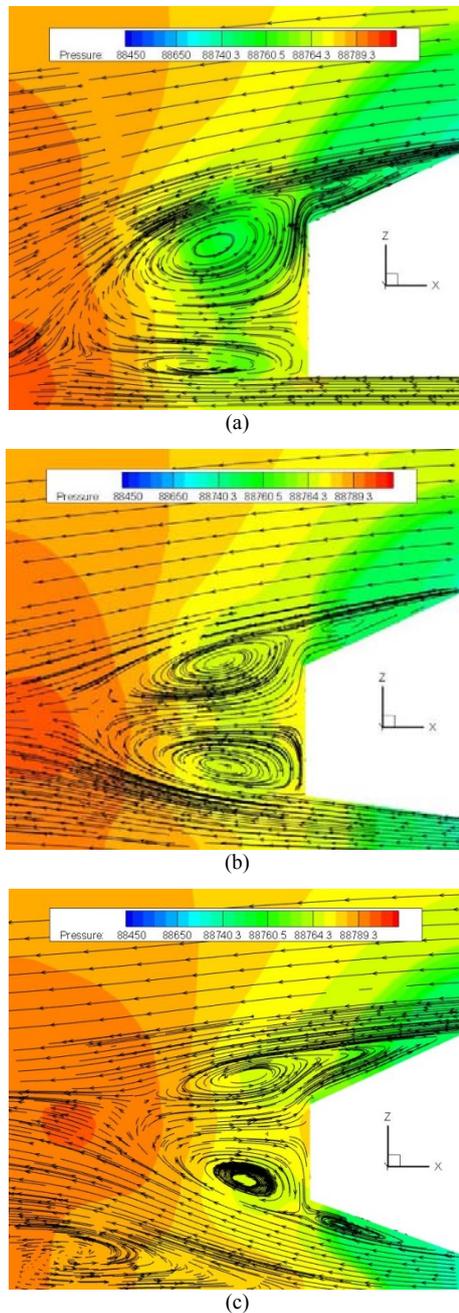
Fig. 12. Flow pattern at the symmetry plane behind the body showing the size of low pressure (recirculating flows), (a): 0 degrees, (b): 8 degrees and (c): 20 degrees- pressure contours in [Pa].

recirculation region has the minimum pressure behind the body. As could be seen in Fig. 12, increasing the diffuser angle leads to decrease in the size of low-pressure regions. A decrement in the size of these areas leads to smaller low-pressure regions behind the body which results in lower drag. But the drag coefficient behavior tends to

increase for larger angles due to other effects which will be discussed here.

Figure 13, shows the flow pattern in the diffuser region for the cases with 8 and 20 degrees diffuser angles. As it can be seen, there is no flow separation at 8 degrees. By further increase in the angle, weak flow separations occur. But for the diffuser angle of 20 degrees, flow completely separates at the diffuser trailing edge which results in complete separation of the flow. In fact, at higher diffuser angles, higher pressure gradients in the diffuser occur. The unfavorable pressure gradients cause the flow separation in the diffuser. These separations create low-pressure regions behind the body, which raises the drag coefficient.

(a)

(b)
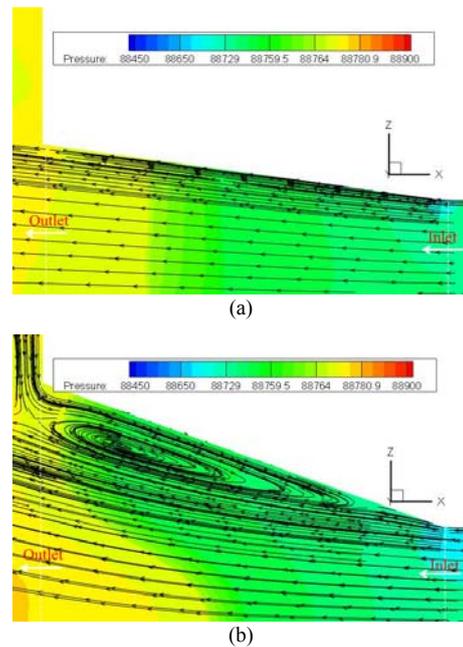
Fig. 13. Flow Separation at higher diffuser (a): 8 degrees and (b): 20 degrees- pressure contours in [Pa].
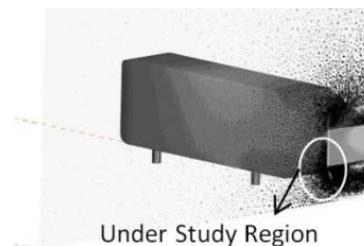
Fig. 14. Location of the longitudinal vortices.

The third phenomenon that must be taken into account is the formation of longitudinal vortices and their growth by increasing the diffuser angle. These vortices are due to flow separations along the side edges of the diffuser (as occurs for slant angle). Since the vortices become massive, the flow topologies could not be studied only in 2D body over a certain point (8°) due to three-dimensional effects. Figure 15 shows the vortices at the region

shown in Fig. 14. As could be seen in Fig. 16, the formation of the vortices becomes more remarkable by increasing the diffuser angle from 8 to 20 degrees. These vortices are low-pressure regions leading to the augmentation of the drag force. Figure 16 shows the vortices' growth with increasing the diffuser angle and pressure drop in the vortex cores. An efficient method to limit the formation of the local longitudinal vortices is to orient simultaneously the flow from the sides of the body in order to retrieve a relative axisymmetric in the after-body flow (Grandemange 2014).

Finally, it is concluded that the drag coefficient is a function of the three factors mentioned. The decrease in the size of the recirculating regions behind the body tends to decrease the drag coefficient while at higher diffuser angles ($\alpha > 8^o$) flow separation occurs beneath the Ahmed body and longitudinal vortices become stronger which causes an increase in the drag coefficient.

(a)

(b)
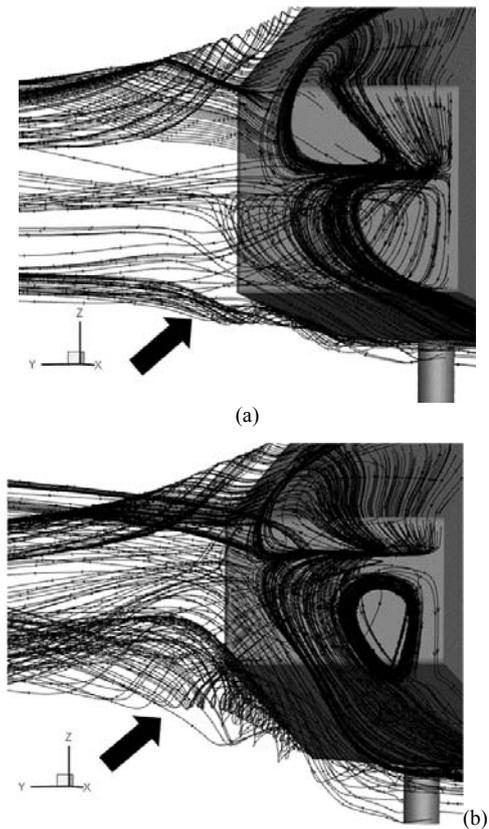
Fig. 15. Formation of longitudinal vortices at the diffuser side edges (pointed by arrows), (a): 8 degrees and (b): 20degrees.

5.2 The Lift Coefficient

Figure 11 (b) shows the descending behavior of lift coefficient while the diffuser angle increases. Even negative lift coefficients are obtained which means the creation of downforce. By checking the pressure contours in the symmetry plane of the diffuser (see Fig. 13), it can be seen that for higher diffuser angles, the pressure at the diffuser inlet decreases (see also Table 6). Pressure drop at the inlet causes

more velocity and mass flow rate under the body. Therefore, the underbody pressure decreases and produces negative lift (downforce).

(a)

(b)
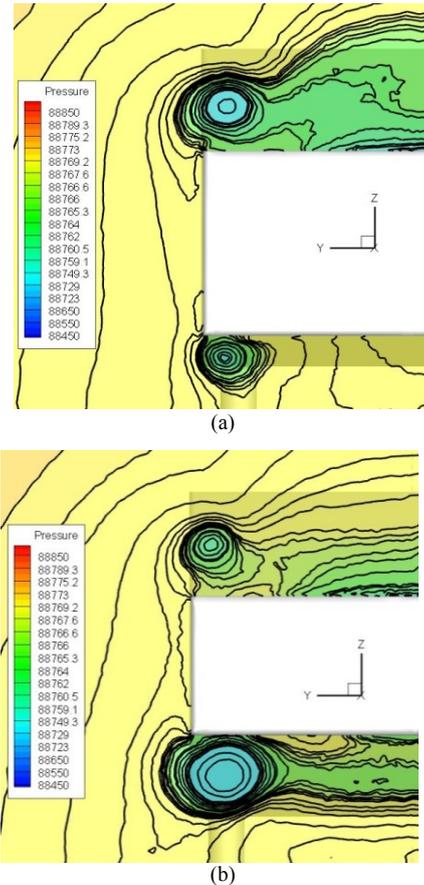
Fig. 16. Growth of the longitudinal vortices and pressure drop in the vortex core shown by pressure contours [Pa] at the diffuser outlet (model rear view), (a): 8 degrees and (b): 20degrees.

For more discussion, the average pressure at the inlet and outlet of the diffuser was calculated (see Fig. 17). The results showed that the outlet pressure (P_2) remains almost constant for all the cases. The results are presented in Table 6. For diffusers with large angles, the outlet area is larger. Therefore, higher pressure differences occur and the inlet pressure will be lower because the outlet pressure is almost constant. In other words:

$$\alpha(\uparrow) \Rightarrow \Delta A(\uparrow) \Rightarrow \Delta P(\uparrow) = P_2(cte) - P_1(\Downarrow) \qquad (6)$$
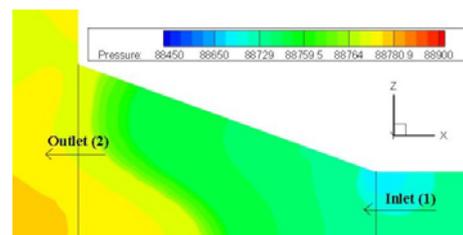
Fig. 17. Calculating the average pressure of shown lines at the diffuser inlet (1) and outlet (2) at the symmetry plane- pressure contours in [Pa].

Where α and ΔA stand for diffuser angle and difference between inlet and outlet area of the diffuser respectively. P_1, P_2 and ΔP are the inlet pressure, outlet pressure and pressure difference in the diffuser respectively.

Table 6 Average diffuser inlet and outlet pressures [Pa].

Diffuser angle	Average inlet pressure (P_1)	Average outlet pressure (P_2)
$\alpha = 0^o$	88767.77	88768.98
$\alpha = 4^o$	88753.37	88782.56
$\alpha = 8^o$	88734.97	88769.36
$\alpha = 12^o$	88725.32	88770.98
$\alpha = 15^o$	88723.98	88772.21
$\alpha = 20^o$	88725.22	88769.70

It is worth mentioning that flow separations in the diffuser reduce the effective outlet area, and this is the reason of the smaller changes in lift coefficient (see Fig. 11(b)) at higher diffuser angles($\alpha > 12^o$).

Figure 18, shows the pressure coefficient (C_p) changes in a diffuser with 8 degrees diffuser angle calculated by:

$$C_p = \frac{p - p_\infty}{\frac{1}{2}\rho V_\infty^2} \tag{7}$$

Where P is the static pressure of the considered location, P_∞ the static pressure in the free stream, ρ the density of the free stream and V_∞ the velocity of free stream. As could be seen, the flow pressure at the inlet section (x=0.02) has the minimum value and by moving through the diffuser, almost reaches the outlet pressure (x=0).
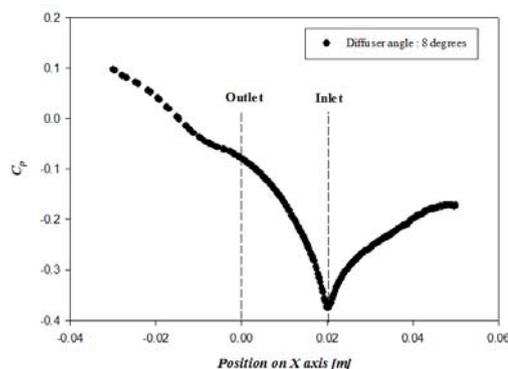
Fig. 18. Pressure coefficient changes along diffuser axis (x) at the symmetry plane from the inlet (x=0.02) to the outlet (x=0).

6. Conclusions

In this paper, it was shown that the diffuser has a great influence on the flow field behind the Ahmed body and can significantly improve the aerodynamic coefficients of lift and drag. Considering a diffuser for the Ahmed model could decrease these coefficients up to 7.3% and 173% for drag and lift respectively and it is noteworthy in comparison with methods have been studied in the literature to decrease the drag. Also, the way that diffuser affects the aerodynamics was investigated in detail. The main findings of the present work are as follows:

- By increasing the diffuser angle, the size of the low-pressure recirculating regions behind the body decreases which individually causes a reduction in the drag force.

- Weak flow separations occur for diffuser angles larger than 8° ($\alpha > 8^o$). At higher diffuser angles (e.g. at $\alpha = 20^o$), flow will be completely separated; therefore, the drag will increase.

- Formation of the longitudinal vortices (at the side edges of the diffuser) would become noticeable for $\alpha > 8^o$. This will cause larger drag forces.

- It was found that the diffuser outlet pressure remains constant. By increasing the diffuser angle, the inlet pressure of the diffuser will decrease. As a result, more air is sucked into the underbody region that produces downforce. However, at higher diffuser angles ($\alpha > 8^o$), flow separations decrease the nominal outlet area of the diffuser which reduces the slope of decrease in the lift coefficient.

- It was concluded from the literature review and the comparison between the studies' results that the optimum angle could be affected by various factors such as vehicle global shape, ground clearance, vehicle speed, underbody design, and probably aspect ratio.

Finally, it is concluded that the optimum diffuser angle must be set empirically to reach the optimum design point based on what really the designer is looking for? (More downforce or just lower drag) which is also affected by vehicle parameters (global shape, underbody design, ground clearance and etc.).

REFERENCES

Ahmed, S. R., G. Ramm, G. Faltin (1984, February 27 –March 2), Some salient features of the time averaged ground vehicle wake, in: *International Congress and Exposition*, Detroit, Michigan, pp.840300.

Aulakh, D. J. S., (2016), Effect of underbody diffuser on the aerodynamic drag of vehicles in convoy, *Cogent Engineering Journal, 3.*

Bayraktar, I., D. Landman, O. Baysal (2001, Nov.) Experimental and computational investigation of Ahmed body for ground vehicle, aerodynamics International Truck and Bus Meeting and Exhibition Chicago, Illinois, SAE Technical Paper Series, 1, 2742.

Beaudion, J. F., O. Cadot, J. L. Aider, K. Gosse, P. Paranthoen, B. Hamelin, M. Tissier, D. Allano, I. Mutbazi, M. Gonzales, J. E. Wesfreid (2004), Cavitation as a complementary tool for automotive aerodynamics, *Exp Fluids* 37, 763-768.

Bruneau, C. H., E. Creusé, P. Gilliéron, I. Mortazavi (2014), Effect of the vortex dynamics on the drag coefficient of a square back Ahmed body: Application to the flow control, European *Journal of Mechanics B/Fluids 45* (2014) 1–11.

Castro, H. G, R. R. Paz, M. A. Storti, Victorio (2010), Experimental and Numerical Studies of the Aerodynamic Behavior of Simplified Road Vehicle, *Mecanica Computacional, XXIX*, 3291-3303.

Cederland, J. and J. Vikström (2010), *The Aerodynamic Influence of Rim Design on a Sports Car and its Interaction with the Wing and Diffuser Flow*, M.Sc. Thesis, Chalmers University of Technology.

Cogotti, A. (1998), A. Parametric Study on the Ground Effect of a Simplified Car Model, *SAE Technical Paper*, pp. 980031.

Corallo, M., J. Sheridan, M. C. Thompson (2015), Effect of aspect ratio on the near-wake flow structure of an Ahmed body Journal of Wind *Engineering and Industrial Aerodynamics, 147*. 95-103.

Fluent 6.3.26 users guide (2015), https//www.Fluent.com.

Grandemange, M., A. Mary, M. Gohlke, O. Cadot (2013), Effect on drag of the flow orientation at the base separation of a simplified blunt road vehicle. *Exp. Fluids 54* (5), (2013b) 1–10.

Grandemange, M., M. Gohlke, O. Cadot (2014), Turbulent wake past a three-dimensional blunt body. Part 2: an experimental sensitivity analysis. *J. Fluid Mech. 752*, 439–461.

Howell, J. P. (1994), *The influence of Ground Simulation on the Aerodynamic of Simple Car Shapes with an Underfloor Diffuser*, Conference on Vehicle Aerodynamics, Royal Aerodynamic Society.

Hu, X., Q. Peng, G. Peng, A. Yang (2011), Effect of Turbulence Parameters on Numerical Simulation of Complex Automotive External *Flow Field, Applied Mechanics and Materials, 37*, 65-69.

Hu, X., R. Zhang, J. Ye, X. Yan, Zh. Zhao (2011), *Influence of Different Diffuser Angle on sedan's Aerodynamic Characteristics*, International Conference on physics Science and Technology (ICPST).

Hucho W. H. (1987), Aerodynamics of road vehicles, *SAE International*, 4th edition, 10-39, 437-458.

Hui, Y. (2006), *A Parametric Study on the Diffuser and Ground clearance of a Simplified Car Model using CFD*, Jilin University.

Huminic, A. and Huminic, G. (2010), *Computational study of flow in the underbody diffuser for a simplified car model*, SAE Technical Paper, No. 2010-01-0119.

Huminic, A., Huminic, G. and Adrian, S., (2012), Study of aerodynamics for a simplified car model with the underbody shaped as a Venturi nozzle, *International Journal of Vehicle Design 58* (1), 15-32.

Kato, Y., N. Horinouchi, S. Shinano (1997), Numerical Investigation of Aerodynamics of Vehicle Underbody with Overset Grid system, *Technical Journal R&D Review of Toyota CRDL, 32*(2), p.23-33.

Katz, J. (1947), *Race Car Aerodynamics*, Bentley publishers, 2nd edition, 152-157.

Khaled, M., H. Elhage, F. Harambat, H. Peerhossaini (2012), Some Innovative Concepts for Car Drag Reduction: A Parametric analysis of Aerodynamic Forces on a Simplified Body, *Journal of Wind Engineering and Industrial Aerodynamics, 107-108*, 36-47.

Lai, Ch., Y. Kohama, Sh. Obayashi, Sh. Jeong (2011), Experimental and Numerical Investigations on the Influence of Vehicle Aerodynamic Drag and Wake Structure, *International Journal of Automotive Engineering*.

Lienhart, H., C. Stoots, S. Becker (2000), *Flow and turbulence structures of the wake of a simplified car model (Ahmed model)*, DGLRFach. Symp. DerAG. ATAB, Stuttgart University.

Mack, S., T. Indinger, N. A. Adams, P. Unterlechner (2012), The Ground-Simulation Upgrade of the TUM Wind tunnel, SAE Technical Paper 2012-01-0299.

Manceanu, R. and J. P. Bonnet (2002), Proceeding of 10th ERCOFTAC (SIG-15)/IAHAR/QNET-CFD *Workshop on Refined Turbulence Modeling*, Poitiers, France.

Meile, W., G. Brenn, A. Reppenhagen, B. Lechner , A. Fuchs (2010), *Experimental and numerical simulations on the aerodynamics of the Ahmed body*, Institute of Fluid Mechanics and Heat Transfer, Graze University of Technology, Austria.

Minguez, M., R. Pasquetti, E. Serre (2009), Spectral vanishing viscosity stabilized LES of the Ahmed body turbulent wake, *Communication in Computational Physics 5*(2-4):635-648.

Rajsinh, Ch., R. Th. K. Raj (2012), Numerical Investigation of External Flow around the Ahmed Reference Body Using Computational Fluid Dynamics, *Research Journal of Recent Science, 1*(9), 1-5.

Rohatgi, U. S. (2012), *Methods of Reducing Vehicle Aerodynamic Drag*, ASME 2012 Summer Heat Transfer Conference Puerto Rico, USA, July 8-12.

Sonawane, P. R., S. P. Sekhawat, K. Rajput (2011), Aerodynamic Analysis of Car Body for Minimum Fuel Consumption, *Journal of Information Knowledge and Research, Mechanical Engineering* 1, 54-57.

Strachan, R. K., k. Knowles, N. J. Lawson (2004, March), *A CFD and experimental study of an Ahmed reference model*, SAE World Congress Detroit, Michigan, vol.1, 0442.

Strachan, R. K., k. Knowles, N. J. Lawson, et al. (2007), The vortex structure behind an Ahmed reference model in the presence of a moving ground plane, *Exp. Fluids, 42*, 659-669.

Tunay, T., B. Sahin, V. Ozbolat (2014), Effects of rear slant angles on the flow characteristics of Ahmed body*, Experimental Thermal and Fluid Science, 57* (2014) 165–176.

Wang, H., Y. Zhou, C. Zou, X. He (2016), Aerodynamic drag reduction of an Ahmed body based on deflectors, *Journal of Wind Engineering and Industrial Aerodynamics, 148* (2016) 34–44.

Wang, X. W., Y. Zhou, Y. F. Pin, T. L. Chan (2013.), Turbulent near wake of an Ahmed model, *Exp. Fluids, 54*(4), 19.